International Journal of GEOMATE, April, 2024 Vol.26, Issue 116, pp.1-10
ISSN: 2186-2982 (P), 2186-2990 (O), Japan, DOI: https://doi.org/10.21660/2024.116.4398
Geotechnique, Construction Materials and Environment

NUMERICAL INVESTIGATION OF CFRP-RETROFITTED CORRODED STEEL I-GIRDER END FOR REMAINING SHEAR AND BEARING CAPACITIES WITH VARIOUS CORROSION PATTERNS

Iola Abi Gail[1], *Tavio[2], and Chien-Kuo Chiu [3]

[1,2]Department of Civil Engineering, Sepuluh Nopember Institute of Technology, Indonesia;
[3]Department of Civil and Construction Engineering, National Taiwan University of Science and Technology, Taiwan

*Corresponding Author, Received: 23 Jan. 2024, Revised: 05 Feb. 2024, Accepted: 6 Feb. 2024

ABSTRACT: Corrosion may cause uniform or localized deterioration to steel bridges, which could gradually diminish carrying capacity as the damage worsens. Carbon fiber reinforced polymer (CFRP) has immense promise due to its low weight and excellent durability, elasticity, and strength. This paper investigates the effectiveness of CFRP as a repair for corroded steel I-girder ends in terms of shear and end-bearing capacities. First, this study presents finite element validation of corrosion and CFRP modeling; based on the result, the setting and analysis process can be implemented in the case study. Then, the simulation of five cases of uniform corrosion involves a range of corrosion damage situations, encompassing corrosion heights, widths, and thickness loss. The stiffener, end web, and inner web simulate the corroded part. Finite element analysis (FEA) uses nonlinearity buckling analysis and assigns the Shell S4R element type steel. The constitutive isotropic elastic model is applied to steel, while CFRP utilizes an orthotropic lamina. The CFRP failure pattern uses the Hashin Damage Criterion model constitutive. Three layers are applied to each side of the model. Analysis shows CFRP in stiffener corroded area significantly increases remaining shear capacity by 0–11.8% for one side and 0–19% for both sides, in bearing capacity by 0–8.4% and 0–17.3%, respectively. Its efficacy in end-bearing is 0–6.3% in the end web, inner web, and combination areas. End web shear capacity increased slightly, while inner and combination web capacity decreased by 0-2% from the health model.

Keywords: Carbon fiber reinforced polymer (CFRP), Corrosion, Disaster risk reduction, Finite element analysis (FEA), I-girder ends, Load-carrying capacity

1. INTRODUCTION

The two main aging issues that progressively shorten the lifespan of steel bridges that considerably diminish the load-carrying capacity are corrosion and live load (fatigue). Web, flange, and stiffener near steel plate girder bridge supports show severe corrosion. This corrosion is primarily caused by the high moisture content, accelerated by inadequate air circulation (especially in the main girder), sediments, depositions, water pools, and antifreeze penetration in the drainage's expansion joint [1,2]. Corrosion may cause uniform or localized deterioration to steel bridges, which could gradually diminish carrying capacity as the damage worsens. Corrosion reduces yield, buckling, and ultimate loads in compression-bending specimens [3,4]. The effects of local corrosion on the bearing, flexure, and shear capacities have been investigated by scholars [5-7]. Zhao et al. [8,9] concluded that location-specific corrosion affected structural load-bearing capacity in corrosion-welded hollow spherical joints with random corrosion.

The relationship between residual capacity and thickness reduction rates in the local corrosion region must be discussed. Further study is required for more accurate elastoplastic behavior prediction of aging steel structures. Additionally, the impact of local web and flange corrosion in the middle stretch has not yet been researched. Repairing corrosion damage usually involves welding or bolting new steel plates to the corroded component or replacing it. However, these methods are costly and impractical. Repairing the deteriorated steel girder ends quickly and efficiently is necessary.

FRP composites are the most preferred material for reinforcing and repairing structures [10-12]. Carbon fiber reinforced polymer (CFRP) is promising due to its lightweight, durability, elasticity, and strength [13-15]. Our nation extensively repairs concrete structures with CFRP. CFRP is rarely used in steel structures; nevertheless, flanges and chord members of steel truss bridges and girder bridges have been coated with CFRP. These parts are generally under normal tension. Cardoso et al. [16] showed that 3 mm thick FRP corrugate-shaped profile reinforcement increased beam strength similarly to 8 mm thick steel plate reinforcements on web surfaces of slender girders at diagonal sections. Pham et al. [17] examined the efficacy of CFRP sheets in reinstating corroded gusset plate connections, and they found that different bonding locations, areas, and directions could restore load-bearing capacity and deformation performance. Elchalakani et al. [18] tested pipes under quasi-static large deformation

using direct indentation and three-point bending. They studied corrosion penetration within the wall thickness, its distribution along the pipe, and the composition and quantity of CFRP sheets. CFRP significantly improves the pipe's flexural and bearing capacity. Yousefi et al. [19] examined circular hollow section (CHS) steel deficient slender columns with and without CFRP strengthening for three corrosion grades at two locations; the retrofitting in externally bonded CFRP fibers under compressive loads increased ductility compared to unwrapped ones. CFRP strengthening slows local buckling and reduces damage stress. Additional research is required to determine the influence of corrosion in the relationship between residual capacity with thickness reduction rate and height corrosion in localized corrosion areas of the steel surface, affecting the efficacy of CFRP laminates in confining corroded I-girder end.

2. RESEARCH SIGNIFICANCE

This paper investigated FEA of the effectiveness of a repair method using the CFRP sheets for the corroded I-girder end. This study simulated the uniform corrosion of five surface patterns. The corroded part location is simulated in the stiffener, end web, and inner web. The modeling involves a range of corrosion damage situations, encompassing corrosion heights, thickness loss, and widths. The influence of this variable on the load-bearing capacity will be clarified. Then, the case study would be retrofitted and bonded with three-layer CFRP sheets to determine the remaining load-carrying capacity value. The numerical study is expanded and verified using the ABAQUS program. Furthermore, the findings of this research could be insight and utilized as a point of reference for future investigations.

3. METHODOLOGY

3.1 Validation of Corrosion Analysis

Nauman Khurram [6] is adopted to verify the analysis process for the corroded model. The primary girder model was a four-panel rectangular plate girder with 1000 mm length and height. The thickness of the web, flange, and stiffeners are 12 mm, 8 mm, and 4 mm, respectively. The stiffener corrosion and internal web damage with a residual thickness within 20 mm damage height and 25% thickness loss were used to validate this paper. The girder model of IWS20t25 (t_s = 2 mm, t_w = 1 mm, and D_h/d = 2%) in the finite element software.

The material steel property is mild steel with a yield stress of 345 MPa, Poisson's ratio of 0.3, and elastic modulus of 210 GPa. The interaction coupling that binds the reference point with the surface area where the load is placed on the steel plate is used. Midspan point loading is applied. The geometry was sufficiently subdivided into parts. A very fine mesh and a mesh size of 2.5 × 2.5 mm and 40 × 40 mm were selected for the corroded region and the girder, respectively.

Table 1 shows that the ABAQUS software force values and journal test results differ by less than 5%. The force-displacement diagram of each model can be seen in Fig. 1. The eigenvalue and deformation results of the elastic buckling analysis in the first mode are 2.15469E+05. The initial deflection, which corresponds to the first buckling eigenvalue mode, is shown in Fig. 2.

Table 1 Validation Result of Comparison

D_{Abaqus} (mm)	D_{Exp} (mm)	P_{Abaqus} (kN)	P_{Exp} (kN)	Difference (%)
3.94502	3.9859	551.429	536.95	2.626

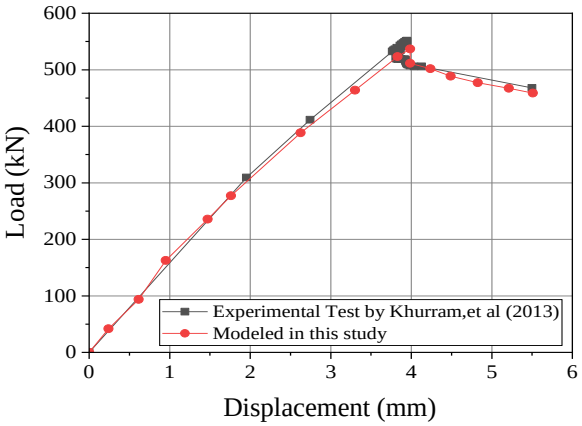

Fig. 1 Force-Displacement Relationship

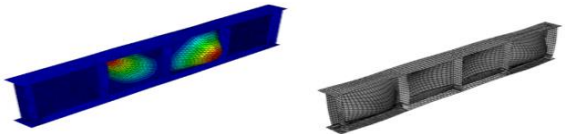

(a) This study (b) Khurram et al. [6]

Fig. 2 Validation model buckling analysis

3.2 Validation of CFRP Analysis

Wakabayashi et al. [14] adopted to verify the analysis process for the CFRP model. The web is 6 mm thick, and the flange and stiffener are 22 mm each. On the left of the panel, steel girder corrosion affects it.

Fig. 3 illustrates the dimensions of the steel girder utilized in the validation model. The yield stress is 300 MPa, Poisson's ratio is 0.3, and elastic modulus E is 200 GPa for a mild steel design using elastic and plastic isotropic materials—the stress-strain plastic used on steel from Bhutto et al. [20]. Elastic lamina components utilized in this validation modeling correspond to the properties of laminated CFRP as

described by Wakabayashi et al. [14] and Daud et al. [21] Table 2.

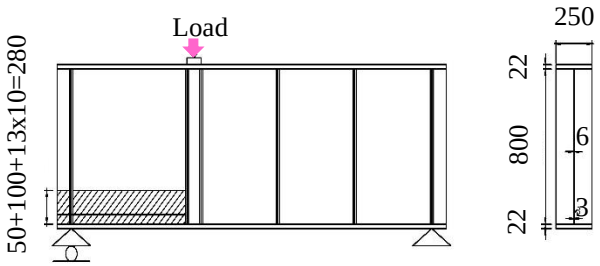

Fig. 3 Dimension of girder [14]

Table 2 Material Properties CFRP

Parts	Elastic Modulus (MPa)
Young Modulus in x_{dir} (E_{11})	640000
Young Modulus in y_{dir} (E_{11})	640000
Shear Modulus in x -y $_{plane}$ (G_{1-2})	6894
Shear Modulus in x -z $_{plane}$ (G_{1-3})	6894
Shear Modulus in y -z $_{plane}$ (G_{2-3})	4136
Poisson Coefficient in x-y_{plane} (v_{1-2})	0.25

Based on Table 3, the difference is 1.55% between the force values obtained ABAQUS software and the force from the test results of Wakabayashi et al. [14]. Fig. 4 shows the force-displacement diagram between this study's force values and Wakabayashi et al. [14] full-bonded analysis force.

Fig. 5 illustrates the initial deflection associated with the first buckling eigenvalue mode. In the first mode, the elastic buckling analysis yielded the eigenvalue and deformation results as 8.1293E+05.

Table 3 Validation result of CFRP validation

Pmax $_{Abaqus}$ (mm)	Pmax $_{Exp}$ (kN)	Difference (%)
1123.09	1105.98	1.55

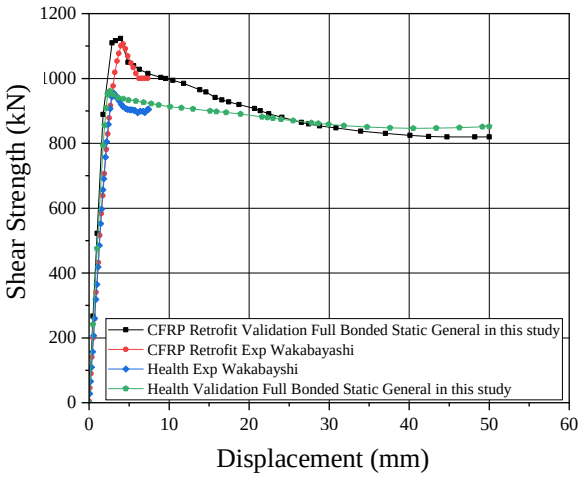

Fig. 4 Force – Displacement Relationship

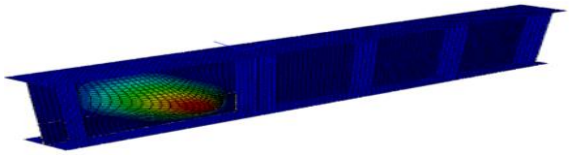

Fig. 5 Initial buckling mode shape (eigenvalue)

3.3 Study Case Analysis

The finite element method was used to analyze the thin-walled composite CFRP retrofitted buckling behavior in ABAQUS. S4R was used to implement the discretization model, which has four nodes and six degrees of freedom (three rotations and three translations) per node and multilayered shell elements. Four nodes in the S4R shell use conventional stress/displacement calculations and reduced integration.

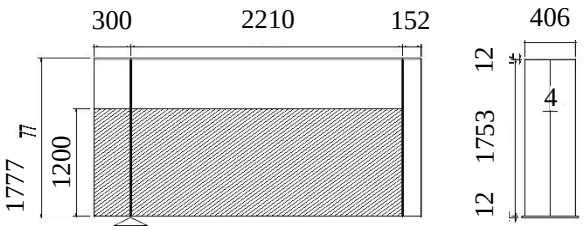

Fig. 6 Dimension and Shape-bonding of the CFRP sheet [22]

The bridge model utilized in this paper is sourced from the U.S. Department of Transportation [22]. Yamaguchi et al. [3] suggested that if the support end's ultimate strength is necessary, the behavior of the entire bridge end can be approximated by 1/4 of the bridge. The span one of the girder section 1 was used to analyze load-carrying capacities, which has a total length of 2662.2 mm and shape bonding, as shown in Fig. 6. The corresponding regulations for highway bridge design in Taiwan mandated, following the specifications of highway bridges in Japan [23], that the length of the web strip for an effect column must be at least 152.4 mm, or 24 times its thickness, in the current instance. Hence, the dimension of the cantilever element utilized in this investigation is 300 mm. The load is applied to the field area to determine the shear capacity of a steel girder. The illustration of the loading is shown in Fig. 7.

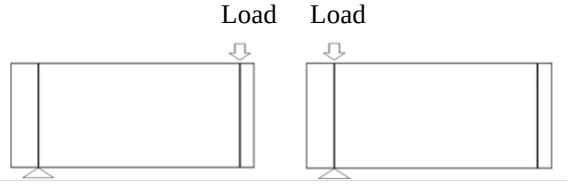

(a) Shear Capacity (b) End-bearing Capacity

Fig. 7 Scheme for Loading

Usukura et al. [21] collected ten corrosion patterns previously identified in studies [1,6,25] for the I-girder end. The corrosion patterns denoted as G1-G5 [21] are predicted by examining corroded steel bridges as described in the referenced research [26]. This strength analysis will review several variables, as described in Table 4. In the height ratio, h represents the corroded height, and h_0 is the height of the corroded part.

Table 4 Schematic of Corrosion Type

Type	Illustration	w/w_0	h/h_0
S1	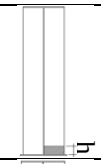	Stiffener Width	0.10 0.25 0.50
S2	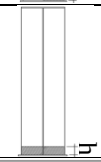	Stiffener Width	0.10 0.25 0.50
W1	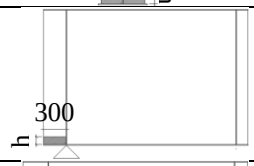	End Web Width	0.10 0.25 0.50
W2	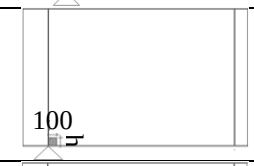	100 mm	0.10 0.25 0.50
W3	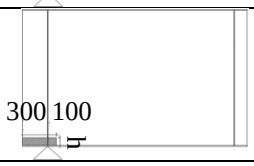	100 mm Inner Web + End Web	100 mm

Three layers were applied to each side of the model (six on two sides). Young's modulus ratio converts the CFRP sheet thickness to steel thickness. Cardoso et al. [16] provided young modulus data, and Wakabayashi et al. [14] provided high-strength carbon fiber with a thickness of 0.121 mm. Wakabayashi et al. [14] review sets the CFRP height with an additional height to cover the corroded section. Thickness $_{CFRP}$ = 0.121 × 220.6 / 200 = 0.133463 mm. The additional height value is 100 + 13 × 10 = 230. If the maximum height of corrosion that occurs at h/h_0 = 0.5 is 876 mm, then the dimensions of the CFRP obtained are: $h_{CFRP} = 876 + 230 = 1116\,\text{mm} \approx 1200\,\text{mm}$. The end web, inner web, and stiffeners of all corrosion patterns repaired with 300 mm, 300 mm, and 203.2 mm CFRP widths have this height. CFRP is continuous along the end web and stiffener. However, due to the corrosion occurring at 100 mm on the inner web, the width of the installed CFRP is identical to that of the CFRP installed on the end web. It is conducted to prevent any wastage of CFRP material. Detail of CFRP installation on corroded area are shown in Fig. 8.

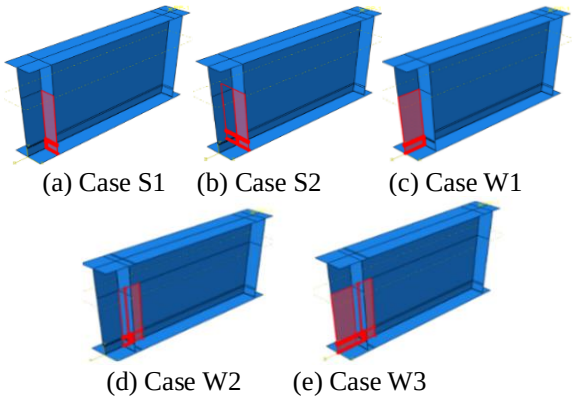

(a) Case S1 (b) Case S2 (c) Case W1

(d) Case W2 (e) Case W3

Fig. 8 Installation of CFRP

Table 5 Steel Properties

Material Properties	ASTM 709 Grade HPS 70W	ASTM 709 Grade HPS 50W
Young's modulus	2×10^5 (N/mm^2)	
Poisson's ratio	0.3	
Yield stress	50 ksi (345 MPa)	70 ksi (483 MPa)
Uniaxial compression material behavior	Bilinear with second slope E/100	
Coefficient of expansion	1.1×10^{-6} (K^{-1})	

Assuming that the material is nonlinear (bilinear), Young's modulus (E) is 2×10^5 N/mm^2, Poisson's ratio is 0.3, and the yield stress of the steel is 50ksi. The slope of the bilinear model's second segment describing materials' behavior under uniaxial compression is E/100. The detailed steel properties are described in Table 5. Table 6 displays the features of the composite profiles derived from the research of Daud et al. [21].

Table 6 Material Properties of CFRP

Parts	Elastic Modulus (MPa)
Young Modulus in x_{dir} (E_{11})	220600
Young Modulus in y_{dir} (E_{22})	22060
Shear Modulus in x -y_{plane} (G_{1-2})	6894
Shear Modulus in x -z_{plane} (G_{1-3})	6894
Shear Modulus in y -z_{plane} (G_{2-3})	4136
Poisson Coefficient in x-y_{plane} (v_{1-2})	0.25

This CFRP failure mechanism uses homogeneous orthotropic laminae (plies) with direction-dependent properties. Deformation in orthotropic materials is usually direction-dependent. An exception arises when forces are exerted in the coordinates that align with the material's natural properties. These

coordinates show lamina points. The transverse coordinate is perpendicular to the fiber reinforcement, while the longitudinal coordinate is parallel. Unidirectionally reinforced composites have longitudinal and transverse axes of symmetry. When loaded in natural coordinates, materials behave like isotropic materials. Normal stresses cause only normal strains, while shear stresses cause only shear strains.

Table 7 Hashin damage criterion parameter

Parts	Elastic Modulus (MPa)
Compressive strength x dir X^C	679
Tensile strength x dir X^T	792
Compressive strength y dir Y^C	71
Tensile strength y dir Y^T	39
Shear strength, S	102

The constitutive orthotropic lamina model is integrated with the collapse mechanism of the Hashin damage criterion for unidirectional fiber composites. This criterion evaluates fracture modes based on stress-component interactions. This criterion was created for unidirectional polymer composites and non-polymeric laminates. The Hashin criteria failure indices pertain to the die and fiber failures and encompass four distinct failure modes. The transverse stress normal component receives maximum stress parameters in three-dimensional problems [27]. The Hashin Damage Criterion parameter is taken from research by Debski et al. [28] shown in Table 7.

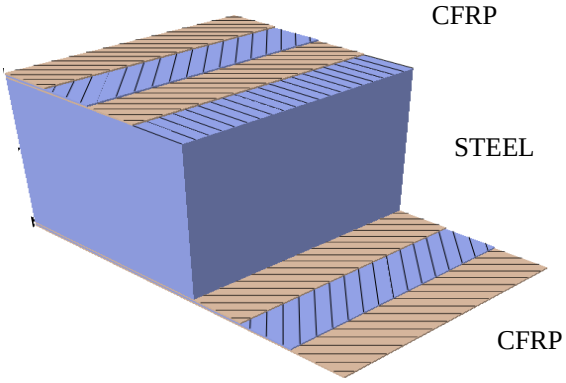

Fig. 9 Composite Layup Setting in ABAQUS

Assuming that the fabric layers were perfectly bonded to the steel and functioned as a homogeneous material, this method is a simplification of the CZM method which is notorious for requiring a great deal of time and CPU resources. The CFRP laminate plate in this study had three layers of unidirectional fiber-reinforced laminate. The laminate was characterized as a quasi-isotropic substance featuring symmetrical layups in a stacking sequence of [0/−45/4]s. The laminate exhibits isotropic surface behavior under in-plane loading, as stated in the material. Retrofitted's laminated composite geometry was represented using composite layup. CFRP and steel have the same thickness and properties. Fig. 9 shows the CFRP laminate model and fiber assignment for the steel plate corroded girder web and stiffener, which had the same plies, thickness, and fiber orientations.

Table 8 and Fig. 10 presents setting boundary-constrained conditions. The modeling utilized in this investigation employs a mesh size of 40 × 40 mm. The dimensions of the corroded region are 5 × 5 mm. A fine mesh was utilized in this investigation to improve force distribution until the degree of precision increased.

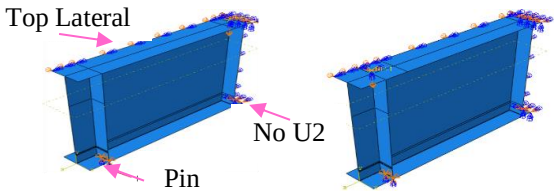

(a) Shear (b) End-bearing

Fig. 10 Boundary Condition

Table 8 Setting Boundary Constrained Conditions

Boundary Condition	U_1	U_2	U_3	U_{R1}	U_{R2}	U_{R3}
Pin	x	x	x	o	x	o
No U2	x	o	x	x	x	x
Top Lateral	x	o	o	o	o	x

o: Free, x: Restrained

4. RESULT AND DISCUSSION

4.1 Effect of Initial Imperfection

This analysis will solely consider the initial deflection analysis conducted using the elastic buckling analysis method. The eigenvalues derived from the elastic buckling analysis of a steel plate girder are presented in Fig. 11. Table 9 presents the value of load-carrying capacity. Load-bearing capacity has been reduced after inputting the initial deflection in the girder modeling.

Table 9 Initial Deflection

Capacity	Pmax without initial deflection (kN)	Pmax with initial deflection (kN)	Difference (%)
Bearing	3353	3144.71	6.62
Shear	3064.12	2830.41	8.26

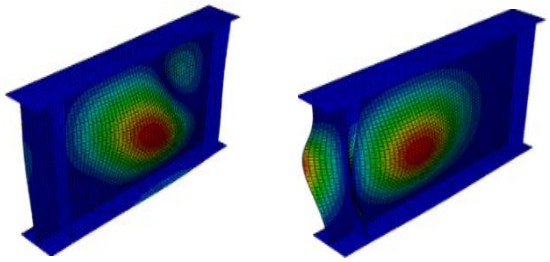

(a) End Bearing capacity (b) Shear capacity

Fig. 11 Bucling analysis

4.2 Health Model Analysis

The health model is the control model that will determine whether a corrosion-affected case model added to a CFRP Sheet increases or decreases in capacity. Fig. 12 presents the load-displacement relationship of the health model. The ultimate load of the health model is 2830.41 kN, while the yield displacement is 12.67 mm, as indicated by the shear capacity (P_o). The subsequently determined value of P_o will serve as a benchmark for control values, which will be assigned a value of 100% (P_u/P_o) regardless of whether the modified model undergoes a corrosion-induced increase or decrease with the addition of retrofit. A comparison will be made between the results of P_u/P_o on the retrofit model and the layer, height, and width parameters for each corrosion thickness loss that occurs on the steel girder bridge of the corroded steel girder model using CFRP in order to assess the effect of the retrofit model.

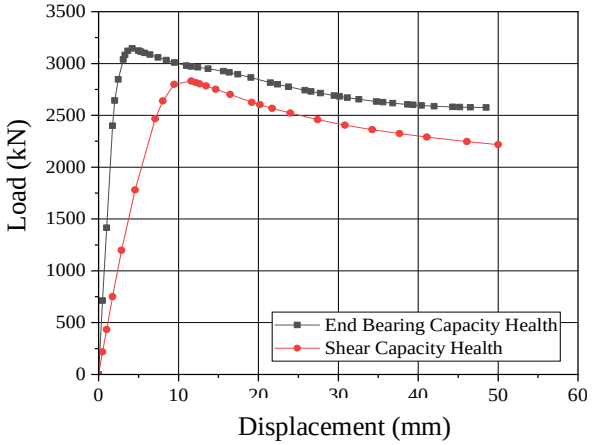

Fig. 12 Load – Displacement of Health Model

4.3 Remaining Shear Capacity

The remaining capacity (Pmax/Pomax) of the corroded modified model without and with retrofit, the remaining capacity of each corrosion pattern, and thickness loss will be compared with the capacity model to determine the effect of CFRP retrofit. Based on Fig. 13, CFRP maintains shear capacity under all conditions in the S1 corrosion pattern. The remaining capacity increase under all conditions h/h_0, in thickness loss conditions of 0 to 10% is a slight improvement of only 0–0.03%, in thickness loss 10 to 25% around 0–4.5%, more significant increases when 25 to 50% thickness loss range 0–11.8%, thickness loss condition of 50 to 75% between 0–6.8%.

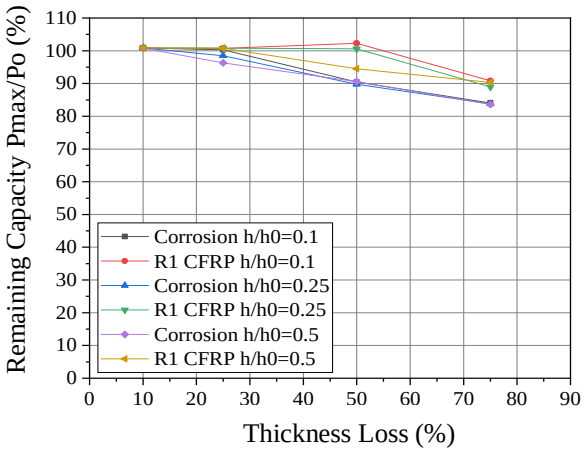

Fig. 13 Remaining shear capacity of S1

The Implementation of CFRP in maintaining shear capacity under all circumstances is effective in the S2 shown in Fig. 14. The increase occurs at all h/h_0 conditions for thickness loss conditions of 0 to 10% is slightly improvement only 0–0.2%; thickness loss of 10–25% significant improvement range 0 to 15.5%. Additionally, when the corroded I-girder end thickness loss is 25 to 50%, the capacity significantly increases around 0–19%, with a thickness loss of 50% to 75% between 0–8,5%.

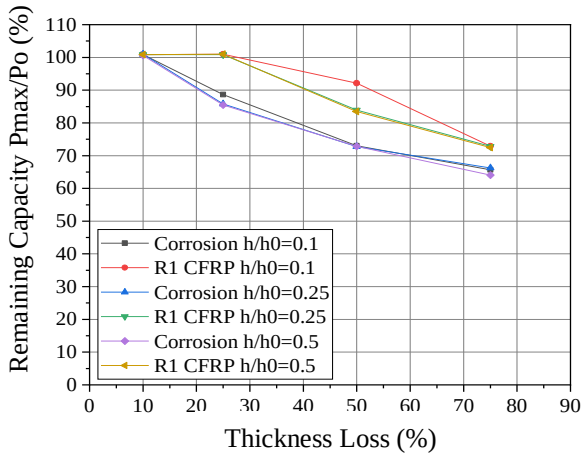

Fig. 14 Remaining shear capacity of S2

Implementing CFRP is slightly effective in maintaining shear capacity in all conditions in the W1, as described in Fig. 15. The capacity increase observed under all height corrosion conditions is

relatively modest, around 0–0.05% for a thickness loss of 0 to 10%, 0–0.12% for a thickness loss of 10 to 25%, 0–1.65% for a thickness loss of 25 to 50%, and 0–3.9% for a thickness loss of 50 to 75%.

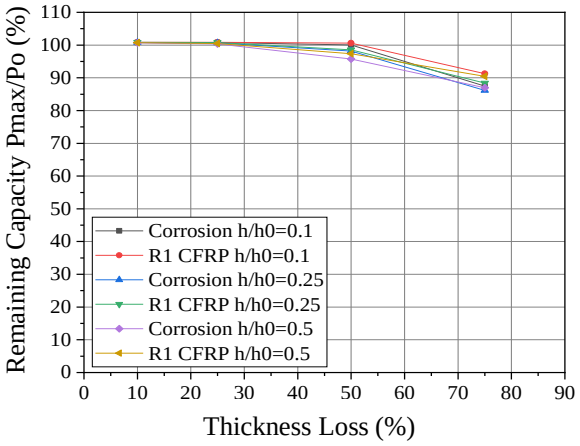

Fig. 15 Remaining shear capacity of W1

Fig. 16 describes the remaining shear capacity on the W2 corrosion pattern. Applying CFRP in the W2 corrosion pattern under 0 to 50% thickness loss in every h/h0 situation improves shear capacity insignificantly. However, it cannot regain its initial capacity with a decrease of 2% from the initial capacity. However, when the thickness loss condition is set to 50 to 75%, the case model to model health improves by 0.9%, 3.8%, and 2.8% for h/h_0=0.1, 0.2, and 0.5, respectively. Hence augmenting the quantity of CFRP layers to accomplish the capacity value.

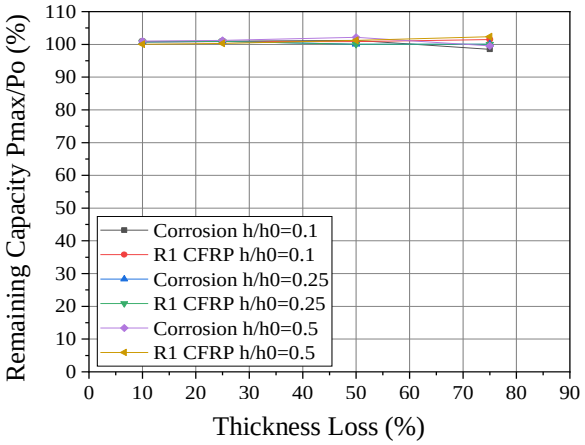

Fig. 16 Remaining shear capacity of W2

The remaining shear capacity of the W3 corrosion pattern can be seen in Fig. 17. Implementing CFRP is marginally effective under all h/h_0 circumstances when the thickness loss ranges from 0 to 10%, indicating a slight substantial increase. It is unable to recover the initial capacity. Therefore, it is suggested that the number of CFRP layers be increased to achieve the initial performance value. In addition, the observed increase is comparatively modest under the condition of thickness loss 10 to 25% ranging from 0–2%, thickness loss 25 to 50% ranging from 0–4.5%, and thickness loss 50 to 75% ranging from 0–5.4%.

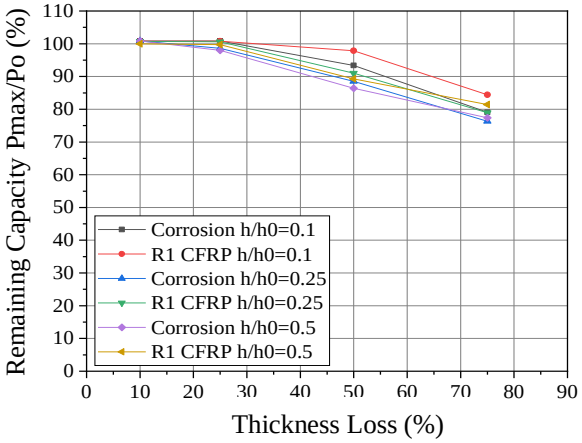

Fig. 17 Remaining shear capacity of W3

4.4 End-Bearing Capacity Analysis

The application of CFRP causes an increase in bearing capacity on the S1 corrosion type, as seen in Fig. 18. The application of CFRP effectively increases the capacity. In all conditions of height corrosion, the capacity increase 0–7.6% in thickness loss 0 to 10%, 0–8.4% in thickness loss 10 to 25%, 0–6.6% in thickness loss 25 to 50%, 0–3.4% in thickness loss 50 to 75%.

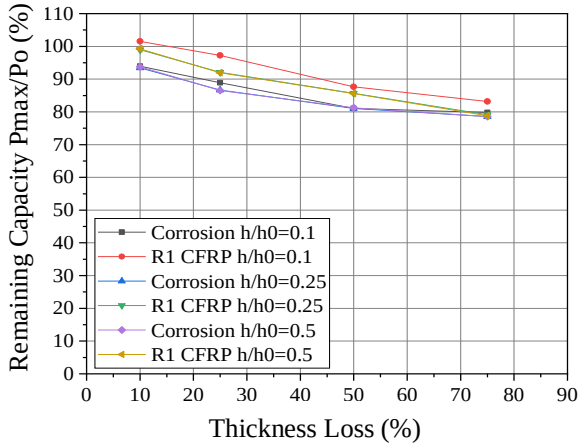

Fig. 18 Remaining end bearing capacity of S1

As depicted in Fig. 19, applying CFRP increases bearing capacity for S2 corrosion types. Under all h/h_0 circumstances, the remaining capacity increases range from 0–14.3% in thickness loss 0 to 10%, thickness loss of 10 to 25% increases around 0–17.3%, when 25 to 50% thickness loss around 0–14.7%, thickness loss conditions are 50% to 75% with a range

of 0–13.5%. Hence, type S2 experienced increased dramatically under all conditions, indicating that applying three CFRP layers is effective in this instance.

The remaining shear capacity of W1 is shown in Fig. 20. The application of CFRP in pattern W1 is slightly enhanced in all circumstances. When thickness loss 0 to 10% range of 0–2.3%, thickness loss 10 to 25% range of 0–1.8%, under the thickness loss condition of 25–50%, the increase is approximately around 0–1.6% and the thickness loss condition of 50 to 75% range of 0–4.3%. It suggests that applying CFRP to increase bearing capacity is marginally effective against corrosion type W1.

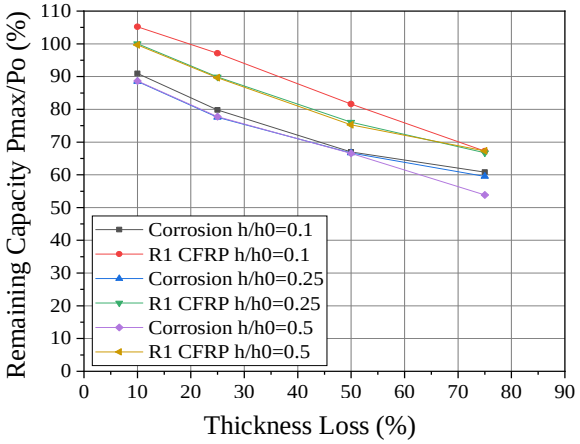

Fig. 19 Remaining end bearing capacity of S2

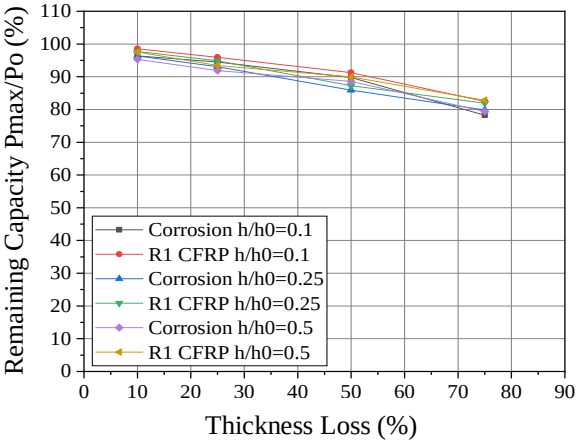

Fig. 20 Remaining end-bearing capacity of W1

As depicted in Fig. 21, the application of CFRP results in a marginal enhancement in bearing capacity under W2 conditions. In corrosion pattern type W2, The implementation of CFRP under all height corrosion (h/h_0) conditions experiences a slight increase of 0–2% in thickness loss conditions of 0 to 25 percent, 0–1.6% in thickness loss conditions of 25 to 50 percent and 0–2.4% when thickness loss conditions of 50 to 75 percent under all height corrosion h/h_0. It is marginally adequate for W2 corrosion types to recover the initial end-bearing capacity.

The remaining end bearing capacity is depicted in Fig. 22. Implementing CFRP in corrosion pattern type W3 effectively recovers the initial performance, although it is a marginal enhancement in the capacity. Improvements that occur are 0–6.3% in thickness loss 0 to 10%, an increase of 0–3.3% in thickness loss of 10 to 25%; an increase ranges from 0–3.7% in thickness loss of 25 to 50%, and around 0–3.6% in thickness loss 50 to 75%, under all height corrosion (h/h0) conditions.

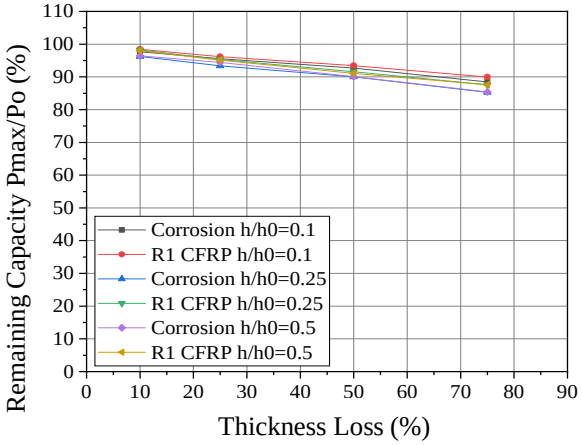

Fig. 21 Remaining end bearing capacity of W2

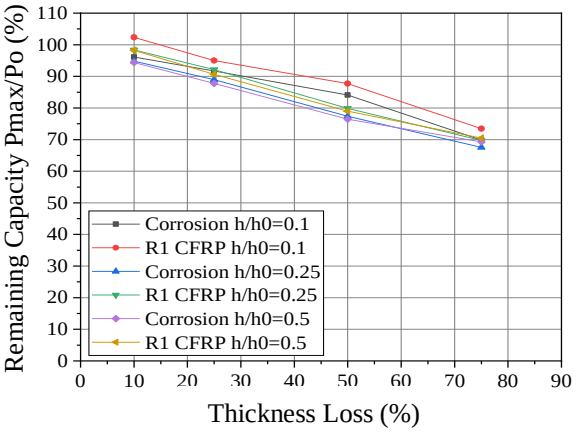

Fig. 22 Remaining end bearing capacity of W3

5. CONCLUSION

Finite element analysis of CFRP-retrofitted corroded steel I-girder ends investigated its effect on corrosion patterns' of shear and bearing capacities.

a. The initial deflection effect on the steel plate bridge is evaluated concerning the end-bearing and shear capacities. Implementing this initial deflection is discovered to diminish the shear and end-bearing capacities. This observation

corresponds to the bridge's actual behavior when subjected to load.

b. The analysis of shear capacity obtained that the application of CFRP is effectively implemented to restore the initial performance of shear capacity in type S1 (single side in stiffener) around 0–11.8%, type S2 (both side stiffener) ranges 0–19%, and type W1 (corrosion in end web) slightly increased by around 0–3.9% in all conditions of thickness loss and height corrosion. On the other hand, type W2 (inner web) under conditions of 10–50% thickness loss and corrosion pattern W3 (end web and inner web) in thickness loss 0 to 10% in every situation of h/h_0 results in an extremely insignificant improvement with decrease around 0-2% and it is incapable of regaining its initial capacity. Hence, it is recommended that the number of CFRP layers be increased to restore the initial capacity of the corroded I-girder end.
c. The end-bearing capacity analysis revealed that adding CFRP in the corroded region significantly increases the remaining capacity of type S1 by 0-8.4%, type W1 by 0-4.3%, and type W3 by 0-6.3%. This improvement is observed across all conditions of thickness loss and height corrosion. Furthermore, the corrosion pattern known as S2 exhibited a significant increase, reaching a range of 0-17.3% under all tested conditions.

6. ACKNOWLEDGMENTS

The authors would like to express their gratitude for the financial support provided by the Institut Teknologi Sepuluh Nopember through the project scheme of the Publication Writing and IPR Incentive Program (PPHKI) 2024. The research was also supported by the international collaboration between ITS in Indonesia and NTUST in Taiwan.

7. REFERENCES

[1] Yamaguchi E., and Akagi T., A Study on Load-Carrying Capacity of Corroded Steel I-Section Girder End, Journal of Structural Engineering, Vol. 59, 2012pp. 80-90, 2013.

[2] Yang M., Kainuma S., Ishihara S., Kaneko A., and Yamauchi E., Atmospheric Corrosion Protection Method for Corroded Steel Members using Sacrificial Anode of Al-Based Alloy, Construction and Building Materials, Vol. 234, 2020, pp. 117405, 2020.

[3] Zhang Z., Xu S., Nie B., Li R., and Xing Z., Experimental and Numerical Investigation of Corroded Steel Columns Subjected to In-Plane Compression and Bending, Thin-Walled Structures, Vol. 151, 2020, pp. 106735.

[4] Jagtap P., and Pore S., Strengthening of Fully Corroded Steel I-Beam with CFRP Laminates, Materials Today: Proceedings, Vol. 43, 2021, pp. 2170-2175.

[5] Tohidi S., and Sharifi Y., Load-Carrying Capacity of Locally Corroded Steel Plate Girder Ends using Artificial Neural Network, Thin-Walled Structures, Vol. 100, 2016, pp. 48-61.

[6] Khurram N., Sasaki E., Katsuchi H., and Yamada H., Finite Element Investigation of Shear Capacity of Locally Corroded End Panel of Steel Plate Girder, International Journal of Steel Structures, Vol. 13, 2013, pp. 623-633.

[7] Xia M., Xu S., Wang Y., Li H., and Zhao B., Experimental Study on Bearing Capacity of Corroded Q345 H-Shaped Steel Column under Axial Compression Load, Journal of Building Engineering, Vol. 52, 2022, pp. 104354.

[8] Zhao Z., Liu H., and Liang B., Probability Distribution of the Compression Capacity of Welded Hollow Spherical Joints with Randomly Located Corrosion, Thin-walled structures, Vol. 137, 2019, pp. 167-176.

[9] Zhao Z., Dai B., Xu H., and Li T., Bending Capacity of Corroded Welded Hollow Spherical Joints with Considering Interaction of Tension Force and Bending Moment, Structures, Vol. 34, 2021, pp. 2656-2664.

[10] Rafani M., Suhardjono A., Wisnumurti, and Wibowo A., A Theoretical Study of GFRP RC Beams Deflection, Journal of Physics: Conference Series, IOP Publishing, Vol. 1477, No. 052047, 2020, pp. 1-5.

[11] Tavio, Rafani M., Raka IG.P., and Ratnasari V., Flexural Capacity Predictions and Comparisons of GFRP Reinforced Beams, Journal of Physics: Conference Series, IOP Publishing, Vol. 1477, No. 052049, 2020, pp. 1-5.

[12] Pinto D., and Raka IG.P., Axial Compressive Behavior of Square Concrete Columns Retrofitted with GFRP Straps, International Journal of Civil Engineering and Technology, IAEME, Vol. 10, No. 1, 2019, pp. 2388-2400.

[13] Chen C., Cai H., and Cheng L., Shear Strengthening of Corroded RC Beams using UHPC–FRP Composites, Journal of Bridge Engineering, Vol. 26, No. 1, 2021, pp. 04020111.

[14] Wakabayashi D., Miyashita T., Okuyama Y., and Koide N., Study on Repair Method using CFRP for Corroded Steel Girder Ends, ed: World Scientific News WSN, Vol. 118, 2019, pp. 181-193.

[15] Al-Ridha A.S., Mahmoud K.S., and Atshan A.F., Effect of Carbon Fiber Reinforced Polymer (CFRP) Laminates on Behaviour of Flexural Strength of Steel Beams with and without End Anchorage Plates, Material Today: Proceeding, Vol. 49, 2022, pp. 2778-2785.

[16] Cardoso H.D.S, Martins J.P., da Silva L.S., and Cimini Jr. C.A., Numerical Study of

Strengthened Slender I-Girders with Fiber Reinforced Polymers, CE Papers, Vol. 3, No. 5-6, 2019, pp. 394-403.
[17] Pham N.V., Miyashita T., Ohgaki K., Hidekuma Y., and Harada T., Repair Method and Finite Element Analysis for Corroded Gusset Plate Connections Bonded to CFRP Sheets, Journal of Structural Engineering, Vol. 147, No. 1, 2021, pp. 04020310.
[18] Elchalakani M., Karrech A., Basarir H., Hassanein M.F., and Fawzia S., CFRP Strengthening and Rehabilitation of Corroded Steel Pipelines under Direct Indentation, Thin-Walled Structures, Vol. 119, 2017, pp. 510-521.
[19] Yousefi O., Narmashiri K., Hedayat A.A., and Karbakhsh A., Strengthening of Corroded Steel CHS Columns under Axial Compressive Loads using CFRP, Journal of Constructional Steel Research, Vol. 178, 2021, pp. 106496.
[20] Bhutto M.A., FRP-Strengthening of Webs of Steel Plate-Girders, Heriot-Watt University, 2014.
[21] Daud R.A., Cunningham L.S., and Wang Y.C., New Model for Post-Fatigue Behaviour of CFRP to Concrete Bond Interface in Single Shear, Composite Structures, Vol. 163, 2017, pp. 63-76.
[22] Grubb M.A., and Schmidt R.E., Steel Bridge Design Handbook Design Example 1: Three-Span Continuous Straight Composite Steel I-Girder Bridge, United States. Federal Highway Administration. Office of Bridges and Structures, 2015.
[23] Association J.R., Specifications for Highway Bridges, Part II, Earthquake Resistant Design, Vol. 228, 1996.
[24] Usukura M., Miyashita T., Sasaki E., Mitsugi Y., Yamazaki T., and Sugiyama T., A Study on Estimation Method of Ultimate Strength of Corroded Steel Girder Ends, Journal of Japan Society of Civil Engineers, Ser. A1 (Structural Engineering & Earthquake Engineering (SE/EE)), Vol. 73, No. 3, 2017, pp. 560-578.
[25] Chiu C.K., Liao I.H., Yamaguchi E., and Lee Y.C., Study on the Simplified Evaluation Method of the Remaining Load-Carrying Capacity of a Corroded Steel I-Girder End using FEA, Journal of Constructional Steel Research, Vol. 210, 2023. pp. 108045.
[26] Tamakoshi T., Nakasu K., Ishio M., Takeda T., and Suizu N., Research on Local Corrosion of Highway Steel Bridges, Technical Note of National Institute for Land and Infrastructure Management, No. 294, 2006.
[27] Chaht F.L., Mokhtari M., and Benzaama H., Using a Hashin Criteria to Predict the Damage of Composite Notched Plate under Traction and Torsion Behavior, Frattura ed Integrità Strutturale, Vol. 13, No. 50, 2019, pp. 331-341.
[28] Debski H., Rozylo P., Gliszczynski A., and Kubiak T., Numerical Models for Buckling, Postbuckling and Failure Analysis of Pre-Damaged Thin-Walled Composite Struts Subjected to Uniform Compression, Thin-Walled Structures, Vol. 139, 2019, pp. 53-65.